NJC

Accepted Manuscript

This is an *Accepted Manuscript*, which has been through the Royal Society of Chemistry peer review process and has been accepted for publication.

Accepted Manuscripts are published online shortly after acceptance, before technical editing, formatting and proof reading. Using this free service, authors can make their results available to the community, in citable form, before we publish the edited article. We will replace this *Accepted Manuscript* with the edited and formatted *Advance Article* as soon as it is available.

You can find more information about *Accepted Manuscripts* in the Information for Authors.

Please note that technical editing may introduce minor changes to the text and/or graphics, which may alter content. The journal's standard Terms & Conditions and the Ethical guidelines still apply. In no event shall the Royal Society of Chemistry be held responsible for any errors or omissions in this *Accepted Manuscript* or any consequences arising from the use of any information it contains.

ROYAL SOCIETY OF CHEMISTRY

www.rsc.org/njc

New Journal of Chemistry RSCPublishing

ARTICLE

One-step synthesis of pure pyrite FeS_2 with different morphologies in water

Binxia Yuan*[a], Weiling Luan*[b], Shan-tung Tu [b] and Jiang Wu [a]

Cite this: DOI: 10.1039/x0xx00000x

Received 00th January 2012,
Accepted 00th January 2012

DOI: 10.1039/x0xx00000x

www.rsc.org/

In the paper, the pyrite FeS_2 with novel nanostructures had been obtained via ethanolamine (ETA)/water binary system. This method provided a uniform and homogenous environment for the nucleation and growth of the FeS_2. When only pure water was used as the reaction solvent, the marcasite FeS_2 with hollow sphere structure was achieved, and then transformed into pyrite phase with rod-like structure piled up by nanoparticles with the increase of reaction time. Moreover, cubic, flake-like, and two kinds of tetrakaidecahedron structures were obtained via the adjustment of volume ratio of ETA and H_2O. The formation mechanism from flower-like amorphous to kinds of morphologies of pyrite FeS_2 crystals was analyzed through the time-dependent controlled experiments. The Raman spectra of samples with different morphologies were investigated, which were consistent with the XRD analysis. The studies of optical properties indicated that the morphologies had a great influence on the absorption properties. This paper provided a very simple and low cost method to control the morphologies of FeS_2 crystals, which would be of great potential for the synthesis of other metal chalcogenides and lay the foundation for the development of the solar cell.

Introduction

Over the past years, there has been considered interest in the synthesis and characterization of transition-metal chalcogenides owing to their excellent optical properties and wide applications in optical cells and devices [1-4]. In particular, iron pyrite (FeS_2) is significantly attractive in both cost and availability comparing with other compounds [5]. Pyrite FeS_2 is applied as photovoltaic cell [6], lithium batteries as a cathode material [7], and hydrogen production as a depolarizer anode [8]. Related reports has proved that pyrite FeS_2 has a high optical absorption coefficient (>10^5 cm^{-1}) and a suitable band gap energy (E_g=0.95 eV) [9-10], indicating potential application on solar cell.

The optical properties of pyrite FeS_2 have a great relationship with their morphologies. For instance, the team of Alivistatos employed a novel single source molecular precursor to obtain pure pyrite FeS_2 nanocrystals, showing quasi-cubic morphologies with a size over 100 nm [11]. The group of Law successfully prepared oblate and spheroid single crystals with diameters of 5-20 nm by a solvothermal process in diphenyl ether media, which estimated the band gap of the NCs as 0.88-0.91 eV [12]. The Wang group first reported synthesis of pyrite FeS_2 with cubic and octahedral shapes via a simple surfactant-assisted ethylene glycol-mediated solvothermal method [13]. Huang's colleagues reported pyrite NCs with cubic shape using a surfactant assisted hot-injection method that yielded pure phase, highly crystalline, and surface stable NCs, indicating the direct optical band gaps was 1.38 eV [14]. The group of Kotov had obtained FeS_2 nanoparticles, nanowires, and nanosheets in polar solvent and aqueous dispersions [15]. Our group had reported the synthesis pyrite FeS_2 with cubic shape (about 100 nm) through oleylamine-mediated solvothermal process, corresponding to a band gap of 1.05 eV [16]. However, most of the synthetic route mainly depended on complex molecular precursor or process route. Here, we adopted the hydrothermal synthesis method in autoclave, which is comparably simple and low cost.

In the paper, we reported a hydrothermal process in an ethanolamine (ETA)/water binary solvent for the synthesis of FeS_2 crystals without expensive single-source precursors and complex craft. The reaction time and the volume ratio of ETA and H_2O played a critical role in the formation of pure pyrite

FeS_2 crystals. In the condition of pure water, the pyrite FeS_2 products weren't obtained. But, interestingly, the hollow sphere shape of marcasite FeS_2 was observed, and which then converted into the rod-like FeS_2 crystals piled up with nanoparticles with the elongation of reaction time. Moreover, the pyrite of four kinds of morphologies, such as, cubic, flake-like, two types of tetrakaidecahedron, also were got. The formation mechanism of these morphologies had also been studied. Accordingly, the Raman and optical properties were measured in order to study the relationship between morphologies and them.

Experimental

Chemicals

All the reactions and operations were carried out in open-air. All chemicals were used directly without further purification. Iron nitrate ($Fe(NO_3)_3$•$9H_2O$, analytical reagent), and ethanolamine (ETA, analytical reagent, 99%)were purchased from Shanghai Chemical Reagent (SCR). Hexadecyl trimethyl ammonium bromide (CTAB, 99%), and L-cysteine ($C_3H_7NO_2S$, 99%) were purchased from Aldrich.

Synthesis of the pyrite FeS_2

In a typical procedure, 1 mmol $Fe(NO_3)_3$ and 5 mmol L-cysteine were added to a given amount of distilled water and were dispersed to form a white emulsion by vigorous stirring. Then, a certain amount of ETA was added into the above solution at room temperature and continually stirred for 15 min to form purple-blue solution. Finally, the resulting mixture was transferred into a Telfon-lined stainless autoclave (60 ml). The autoclave was sealed and maintained at 200 ^oC for 48 h, then cooled to room temperature naturally. After that the resulting black solid products were collected by centrifugation, washed with alcohol to remove the excess surfactants, and finally dried naturally as well as utilized for further characterization.

Characterization

X-ray diffraction (XRD) patterns were recorded with a Rigaku D/max 2250 V diffractometer operating with Cu Kα radiation. The operation voltage and current were set as 40 kV and 100 mA, respectively, and the samples were powder without further treatment. Field emission scanning electron microscope (FESEM) images were acquired using S-4800 operated at an acceleration voltage of 10 kV, and the samples were prepared by sonicating the products in absolute ethanol, then evaporating one drop of suspension on conductive adhesive. The Raman spectra were recorded on InVia-Reflexa Raman spectrometer operating with 512 nm laser. The absorption properties were acquired by Cary 500 UV-vis-NIR spectrophotometer, the samples were provided by sonicating the samples in ethylene tetrachloride (C_2Cl_4).

Results and discussion

Structures and morphologies

In our experimental, a homogenous reaction condition for the nucleation and growth of the product was provided. It was found that synthesis of FeS_2 particles with controlled morphologies could be obtained by adjusting the experimental conditions, such as reaction time or the volume ratio between ethanolamine and water. The obtained morphologies of FeS_2 particles were summarized in Table 1.

Table 1 Summary of various morphologies of the FeS_2 samples

Sam-ple	Phase	V_{ETA}: V_{H2O}	Tempera-ture/^oC	Tim e/h	Morpholog y
A	pyrite	8:1	200	48	cubic
B	pyrite	1:1	200	48	flake-like
C	pyrite	1:8	200	48	tetrakaideca -hedron
D	marcasite	pure water	200	24	hollow sphere
E	pyrite and marcasite	pure water	200	48	rod-like

The phases of the as-prepared samples were characterized by XRD, as shown in *Fig. 1a*. All diffraction peaks of *samples A, B and C* could be indexed as a pure cubic phase of FeS_2 (space group Pa3) with a lattice constant of 5.4287 Å, which is consistent with the value given in the standard card (JCPDS no. 42-1340). No impurities were detected, indicating the high purity of the as-synthesized samples. Moreover, the strong and sharp diffraction peaks implied their high crystalline structure. The crystal structure of pyrite FeS_2 is displayed *Fig. 1b*. The Fe^{2+} cations occupy the sites of a face-centered-cubic sublattice, and the $(S_2)^{2-}$ dimers are centered at the midpoints of the cubic edges and body center, so that the phase-structure can be considered as NaCl-like. The axes of the $(S_2)^{2-}$ dimers are oriented along the [111] directions; each Fe atom is coordinated by six sulfurs in a slightly distorted octahedron and each S atom

is bonded to three Fe atoms and its dimer pair.

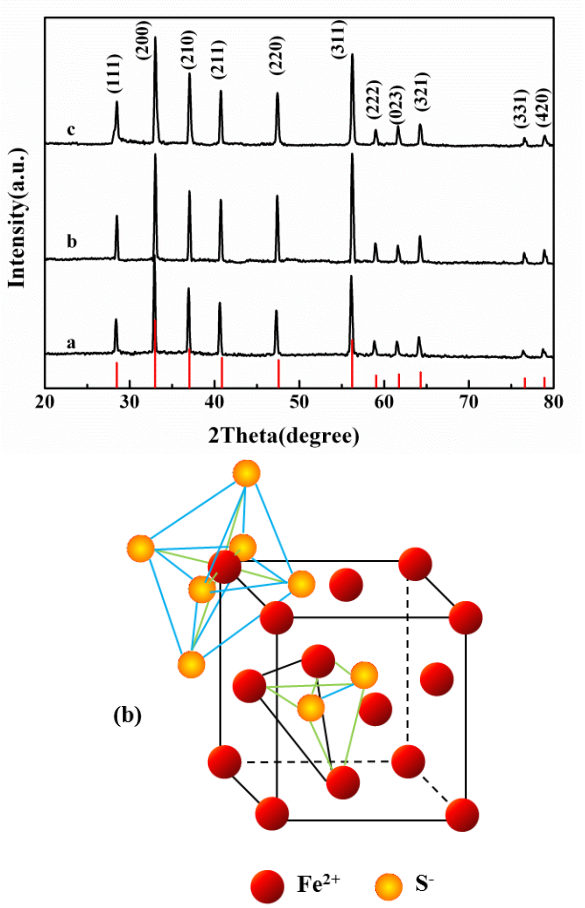

Fig. 1. XRD patterns of FeS_2 crystals obtained under different conditions: (a) *sample A*, V_{ETA}: V_{H2O}=8:1; (b) *sample B*, V_{ETA}: V_{H2O}=1:1; (c) *sample C*, V_{ETA}: V_{H2O}=1:8, with reaction for 48 h at 200 ^{o}C, (b) the crystal structure of pyrite FeS_2.

To obtain the morphology and size information of as-prepared FeS_2 samples, the technique of SEM was employed. The SEM images (*Fig. 2*) depicted various crystals in different volume ratio of solvents at 200 ^{o}C for 48 h. When the volume ratio of ETA and H_2O (*sample A in Table 1, Fig. 2a*) was adjusted to 8:1, as shown in *Fig. 2a*, cubic-like FeS_2 particles with length of 400 nm were clearly observed. By simply decreasing the volume ratio of ETA and H_2O to 1:1 (*sample B in Table 1, Fig. 2b*), desultorily flake-like were obtained as presented in *Fig. 2b*. Interestingly, ployhedron shape was formed when the volume ratio of ETA and H_2O was reduced to 1:8 (*sample C in Table 1, Fig. 2c)*. To further understand the morphology difference, it was worthwhile to investigate the change of relative intensity in each crystal lattice. Table 2 listed the crystals strength of different morphologies FeS_2 samples obtained under various reaction conditions. From the table, it could be found that the intensity values of *sample A* and theoretical sample in each lattice plane were essentially identical, which meant that *sample A* didn't have orientated growth along specific crystal. With the increase of H_2O content (V_{ETA}: V_{H2O}=1:1), the strongest peak became (311) crystal plane. This proved that the (311) crystal face was dominant and had more chances to be diffracted, which indicated *sample B* grew up along (311) plane. This result was coincided with the SEM images with flake-like structure. When the volume ratio of ETA and H_2O was reduced to 1:8, the position of three strong peaks had no change and there were an increase in the relative intensities of (210), (220) and (023) crystal planes comparing with other planes. More investigation would be explained in detail later in this article.

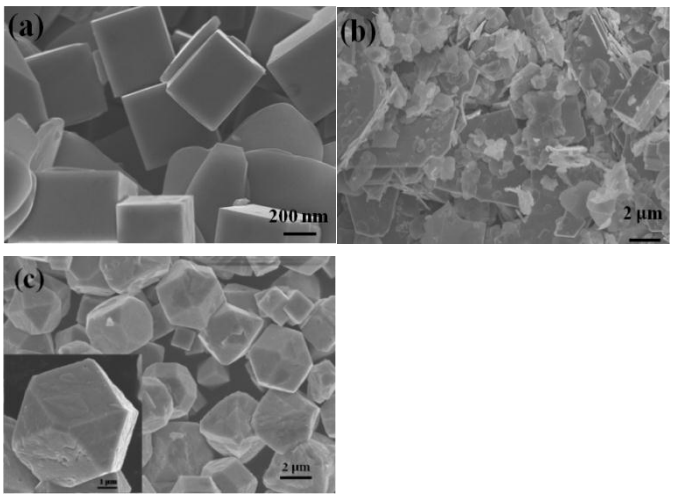

Fig. 2. SEM images of FeS_2 crystals obtained under different conditions: (a) V_{ETA}: V_{H2O}=8:1; (b) V_{ETA}: V_{H2O}=1:1; (c) V_{ETA}: V_{H2O}=1:8, with reaction for 48 h at 200 ^{o}C

Table 2. The relative intensities of crystal faces in measurement and theory

Crystal face	Sample			Theoretical model
	A	B	C	
(111)	35.0	41.3	38.1	31.0
(200)	100.0	98.2	100.0	100.0
(210)	57.7	60.6	66.0	53.0
(211)	53.5	53.2	50.4	40.0
(220)	45.7	60.9	48.8	36.0
(311)	72.5	100.0	71.2	69.0
(222)	14.8	16.6	13.9	11.0
(023)	15.8	15.5	18.2	13.0
(321)	8.2	24.0	19.3	16.0

Under the reaction condition without ETA and the original molar ratio of iron and sulfur sources being 1:5, although CTAB phase catalyst (0.01-0.5mmol) was added and the reaction time was prolonged, the pure pyrite FeS_2 phase cannot be obtained. Generally, long reaction time leads to a preference for the formation of a thermodynamically stable phase. Therefore, marcasite FeS_2 was appeared first. With the extension of reaction time, marcasite would gradually transform into pyrite FeS_2. *Fig.3* showed the evolution of XRD patterns from marcasite to pyrite FeS_2. When the reaction time was kept as 24 h, marcasite FeS_2 was the main product with a small amount of pyrite FeS_2. By Rietveld refinements from the XRD patterns, the weight of marcasite FeS_2 accounted for 71.4%, and the weight of pyrite FeS_2 was 28.6%. According to the XRD pattern, the characteristic peaks of pyrite FeS_2 (65.7% w.t.) accounted for the majority after 48 h, but marcasite FeS_2 (34.5% w.t.) could still be observed in the sample. Obviously, the transform process was quite slowly, the marcasite FeS_2 phase persisted after a long reaction time. Thus, it was difficult to obtain pure pyrite FeS_2 phase in the reaction system without ETA.

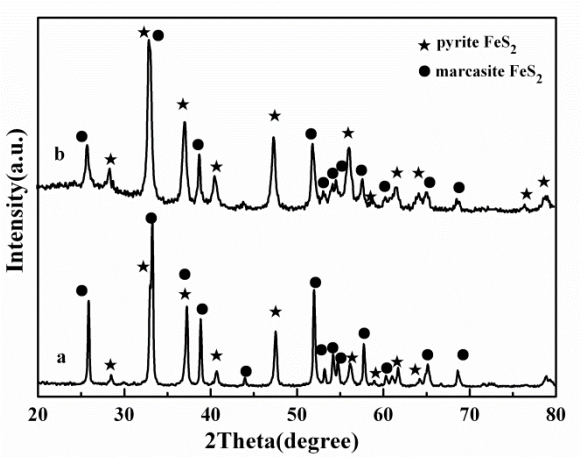

Fig. 3. Evolution of the XRD patterns with different reaction time (a) 24 h, (b) 48 h, reaction temperature is 200 ^oC

To further investigate the conversion process from marcasite to pyrite FeS_2 occurring at pure water, SEM analysis was conducted to characterize the samples at different conversion steps, as shown in *Fig. 4*. A hollow sphere of marcasite FeS_2 crystals was observed in *Fig. 4a*. The inserted panel in *Fig. 4a* was magnified single hollow sphere typically accumulation of many nanoparticles. When the reaction time was increased to 36 h, the morphologies of samples were still sphere structure (*Fig. 4b*), but a portion of hollow spheres became composed of rod-like by orderly particles. It implied that the marcasite phase was converting towards pyrite phase structure. Interestingly, when reaction time was further extended to 48 h, the sphere particles disappeared while rod-like ones appeared (*Fig.4c and 4d*). The rod-like particles were piled of many nanoparticles, with a length of about 500-600 nm and a diameter of about 100 nm.

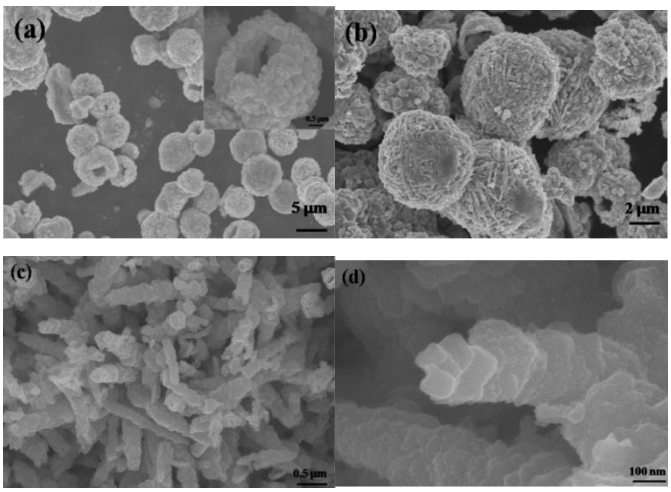

Fig. 4. SEM images of FeS_2 crystals under the different reaction time: (a) 24 h; (b) 36 h; (c) and (d) 48 h, synthesis in pure water.

It was worthwhile to study the transformation process of from marcasite hollow sphere to pyrite rod-like. Based on diffusion and thermodynamic processes, the formation process of hollow spheres and phase transformation was discussed. On the thermodynamic, the stability of pyrite phase was higher than marcasite phase. According to free energy (G) vs. temperature (T) graph in allotropic transformation[17], at a relatively low reaction temperature, marcasite and pyrite FeS_2 simultaneously grow in a competitive process. At the beginning of the reaction, the concentration of marcasite FeS_2 monomer (single FeS_2 molecule before its nucleation and growth) became increasingly higher, which lead to a high crystallization and growth rate. At the time when both Fe and S sources were consumed, the precipitation-solubility equilibrium of FeS_2 in solution became the main process. With extending of reaction time, thermodynamic control became the major factor and marcasite FeS_2 gradually converted to the thermodynamically stable phase of pyrite FeS_2.

As depicted in *Fig. 5*, at first the marcasite nuclei was acquired (step 1), these small particles agglomerated together to form larger hollow sphere clusters (steps 2 and 3), the allotropic

transformation of FeS_2 from marcasite to pyrite phase began to appear (steps 4 and 5), and rod-like pyrite was ultimately acquired via Ostwald ripening (step 6). Several reports [18-21] had stated the relevant theoretical and experimental analysis of formation of hollow sphere. At the early stage, it was the surface diffusion along the early formed hollow walls. The diffusion was then thermodynamically driven by controlling the direction of the reaction. And the formation of hollow structures was thermodynamically instability in the long run. Compared with the hollow sphere structure, the rod-like structure had a higher stability. As a result, the hollow sphere finally reduced the empty space to minimize the interface energy. By controlling the atomic concentration and further collective ways of initial nuclei and diffusion properties of different ions, structural design for driving force could be acquired under a set of experiment parameters. Thus, studies of the synthetic mechanism of hollow sphere and phase conversion with the above investigations will be the great challenge in our future research.

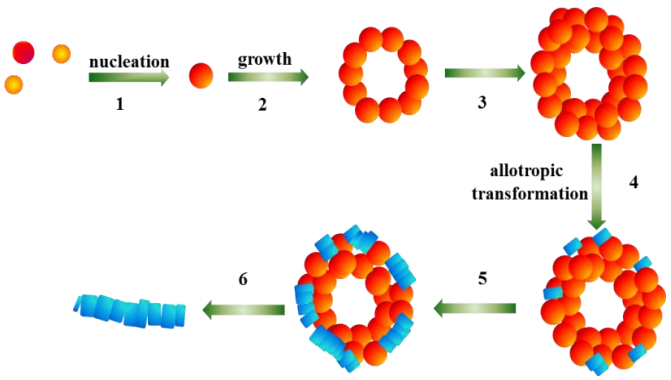

Fig. 5. Transformation mechanism of from hollow sphere to rod-like: formation process of marcasite nuclei (1), aggregation of nanocrystllites into single-hollow sphere (2 and 3), allotropic transformation (4 and 5), and creation of a rod-like via Ostwald ripening (6).

In the meantime, the FeS_2 phase couldn't be obtained if $Fe(NO_3)_3$•$9H_2O$ was replaced by $FeSO_4$ $7H_2O$ or Fe_2O_3 under other conditions kept unchanged. If using elemental sulfur as sulfur source, the acquired crystals were Fe_3S_4 samples. The control experiments showed that the choices of iron sources, sulfur sources, and solvents were critical for the obtaining of different phases and morphologies FeS_2.

Time-dependent experimental. In order to study the growth mechanism of FeS_2 crystals, a series of experiments were performed with different reaction time.

In the synthesis of cubic-shape pyrite FeS_2, the ideal reaction temperature and volume ratio of ETA and water were adjusted to 200 ^oC and 8:1, respectively. *Fig. 6* showed the SEM images of samples obtained at different time intervals. When the reaction time was kept as 1 h (*Fig. 6a and 6b*), a large number of uniform flower-like microspheres with a diameter about 500 nm were observed. XRD results proved the sample obtained at 1 h was amorphous. When increasing the reaction time to 12 h (*Fig. 6c*), the as-obtained sample was comprised of mixture of a large amount of stripe-like (length: 200-600 nm, width: 100 nm) with some small flake-like (about 100 nm). XRD analysis confirmed this result with "steamed bread" peak and three weak diffraction peaks of pyrite FeS_2. When the reaction time was further extended to 24 h, the product was confirmed to be pyrite FeS_2 crystalline based on XRD with flake-like particles (*Fig. 6d*). When the reaction time was extended to 36 h (*Fig. 6e*), the flake-like started to become thick with a small quantity of cubic-shape FeS_2 appeared. While further prolonged the reaction time to 48 h (*Fig. 6f*), the flake-like samples almost transformed into cubic-shape structure with a side length about 400 nm.

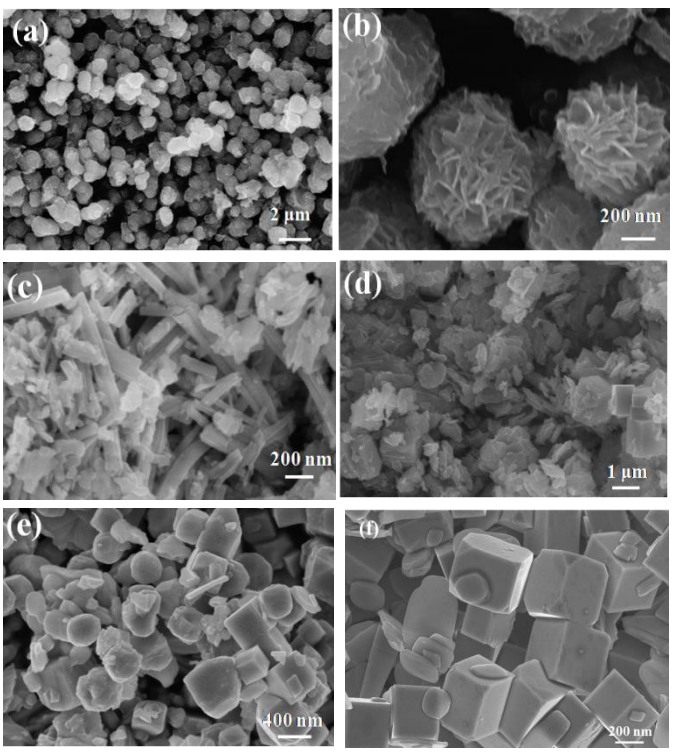

Fig. 6. SEM images for the shape-evolution process of FeS_2 crystals under different reaction time in V_{ETA}/V_{H2O}=8:1: (a, b) 1 h; (c) 12 h; (d) 24 h; (e) 36 h; (f) 48 h

On the basis of the above investigation, the growth process

of the pyrite FeS_2 cubic-shape microparticles could be classified following two steps: an initial nucleating stage and a crystal growth stage, which involved a fast nucleation of amorphous primary particles followed by a slow aggregation and crystallization of primary particles. Firstly, because L-cysteine consists of $–NH_2$, –COOH, and –SH functional groups, they have a tendency to coordinate with inorganic cations. Therefore, it was reasonable to conclude that L-cysteine reacted with free Fe^{3+} to form relatively stable Fe-cysteine complex. With the extension of reaction time, system energy increased, flower-like microsphere Fe-cysteine complex became unstable, leading to flower-like microsphere decomposed and formation of pyrite FeS_2. When there is enough reaction time, the Fe-cysteine completely decomposed to form FeS_2 nuclei for later growth. It is generally regarded that with prolonged reaction time, the morphologies of sample would convert into the structure with small surface energy. For a cubic face-centered structure, the surface energy is considered to be in the order {111} < {100} < {110}, and the growth preferentially.

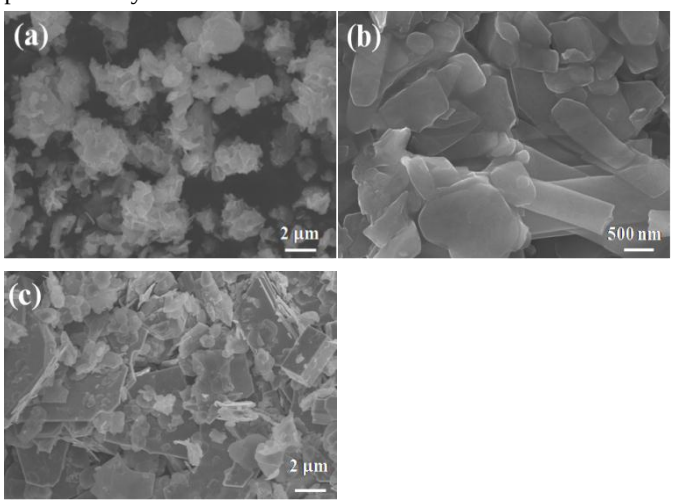

Fig. 7. SEM images for the shape-evolution process of FeS_2 crystals under different reaction time in V_{ETA}/V_{H2O}=1:1 (a) 24 h, (b) 36 h, (c) 48 h

In the synthesis of flake-like pyrite FeS_2 crystals, the volume ratio of ETA and H2O is 1:1. *Fig. 7* showed the SEM images of the samples obtained at different time intervals. These samples were indexed as pyrite FeS_2 crystal by XRD analysis. When the reaction time was 24 h (*Fig. 7a*), a large number of irregular micro-particles were observed. When the reaction time was extended to 36 h (*Fig. 7b*), the morphologies of crystals were slice-like. A further increasing reaction time to 48 h, the final products exhibited thin plate morphologies of a broader size distribution.

When the volume ratio of ETA and H_2O was adjusted to 1:8, the change of morphologies was quite interestingly and worthy of investigation, as shown in *Fig. 8.* At 24 h (*Fig. 8a and 8b*), a large number of flocculent structure constructed from curved nano-flakes and a few bulk structures were observed. When the reaction time was increased to 30 h (*Fig. 8c*), the as-prepared sample was comprised of a large amount of cubic-shape with different sizes. When the reaction time was further increased to 36 h (*Fig. 8d*), the products consisted of lots of tetrakaidecahedron. While the reaction time was extended to 48 h (*Fig. 8e*), the tetrakaidecahedron structure was different and had a change.

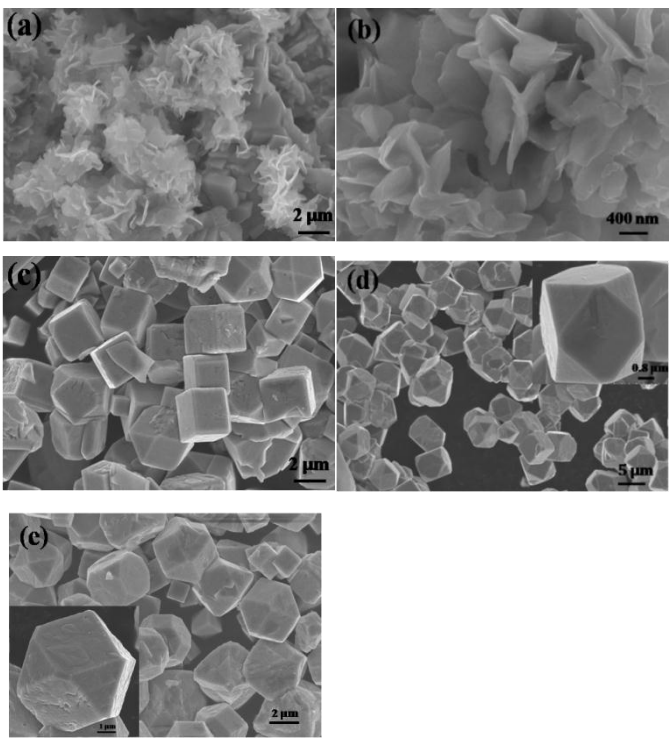

Fig. 8. SEM images for the shape-evolution process of FeS_2 crystals under different reaction time in V_{ETA}/V_{H2O}=1:8 (a, b) 24 h, (c) 30 h, (d) 36 h, (e)48 h.

On the basis of the experimental results and analyses, the entire formation process of nucleation growth, oriental assembly, and subsequent cubic-deformation was proposed to illustrate the growth mechanism. At the initial stage of hydrothermal reaction, free Fe^{3+} could coordinate with L-cysteine to form Fe-cysteine precursor which then decomposed to FeS_2 nuclei. Then the flocculent morphologies were immediately obtained due to the effect of water and

further cubic-shape FeS_2 crystals were got owing to the effect of ethanolamine. Table 3 showed the relative intensities of FeS_2 crystals in different crystal plane. When the reaction time was shorter than 30 h, the relative intensities of FeS_2 crystals in different crystal panel were close to the theoretical value. Although the shapes of inorganic materials often conveyed their intrinsic crystal structure nature, crystals can display diversiform morphologies under the influence of extrinsic environmental factors. The behavior leaded to distinct surface energies, directly resulting in different growth rates of the crystal face. Herein, the morphology of FeS_2 sample was subtly predominated by the facet-selective adsorption characteristic of ETA, which serves as a structure-directing coordinate template. Moreover, ETA acts as a phase catalyst in this system. According to the SEM images (*Fig. 8c, 8d, and 8e*), the sizes of samples remained unchanged about 3 μm with the increase of reaction time. The results indicated that the particle didn't grow large but with morphology transformation by prolonging reaction time. When the reaction time was 36 h, the relative intensity of (111) crystal plane was greater than the sample prepared at 24 h and 30 h. It was indicated that the (111) crystal face had more chance to be diffracted, which meant the phase structure or morphology had changed a little. At 48 h, the intensity of the same plane was decreased but those of (210) and (023) showed a certain degree of increase, indicating a dominant role with the increase of reaction time. In order to further understand the formation process, the possible schematic diagram was shown in *Fig. 9*.

Table 3. The relative intensities of the different crystal faces (V_{ETA}/V_{H2O}=1:8)

Crystal indices	sample				Theoretical model
	24h	30h	36 h	48h	
(111)	37.2	36.4	41.0	38.1	31.0
(200)	100	100	100.0	100.0	100.0
(210)	54.7	55.3	56.3	66.0	53.0
(211)	48.9	49.1	50.1	50.4	40.0
(220)	46.2	46.7	47.2	48.8	36.0
(311)	72.3	71.6	70.8	71.2	69.0
(222)	12.8	12.1	12.7	13.9	11.0
(023)	15.8	14.3	14.8	18.2	13.0
(321)	18.0	19.1	20.5	19.3	16.0

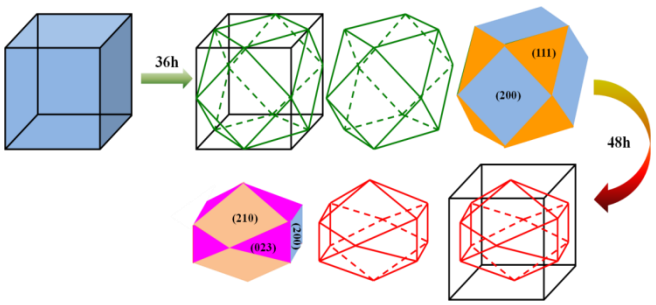

Fig. 9. Schematic illustration of the proposed formation mechanism of FeS_2 crystals

Raman and optical properties of FeS_2. The Raman spectra of the FeS_2 samples obtained at different reaction conditions were showed in *Fig. 10*. Generally, high-purity, crystalline FeS_2 with pyrite structure usually exhibits three characteristic Raman peaks at 340-353 cm^{-1} (E_g, T_g), 377-383 cm^{-1} (A_g, T_g), and 427-466 cm^{-1} (T_g) [22-23]. The peak at 340 cm^{-1} was E_g mode which the sulfur atoms are displaced perpendicularly to the dimmer axes, the peak at 377 cm^{-1} was A_g mode which corresponds to in-phase stretching vibration of the S-S dimmer of pyrite FeS_2. Moreover, no other peaks were observed. Thus, the Raman results further indicated *samples A, B*, and *C* were of pure pyrite structure without marcasite FeS_2 or other impurities. On the contrary, the Raman peaks of *sample D* were located at 323 cm^{-1} and 385 cm^{-1}, indicated a marcasite phase instead of pyrite. While the Raman spectrum of *sample E* showed three peaks at 323 cm^{-1}, 340 cm^{-1} and 377 cm^{-1}, revealing a mixture of pyrite and marcasite FeS_2. Based on the above analysis, the phase structures of as-prepared samples were further proved, in agreement with XRD analysis.

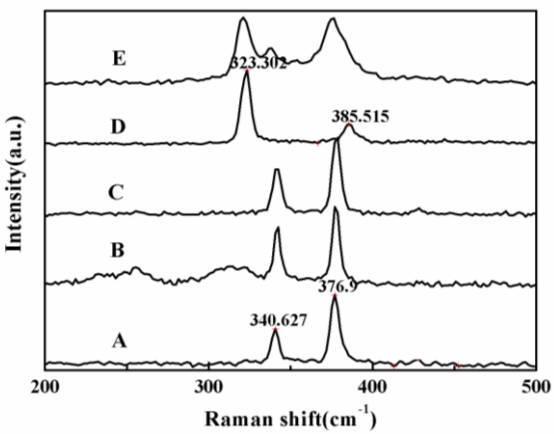

Fig. 10. Raman spectra of products obtained in the different samples *A, B, C, D, and E*.

The optical properties of FeS_2 dispersed in ethylene

tetrachloride (C_2Cl_4) by sonication were studied at ambient temperature absorption spectroscopy from 300 nm to 2500 nm, as shown in *Fig. 11*. It was found that absorption properties are quite different among the samples because of their diverse morphologies. Although samples A, B, and C were all pyrite FeS_2 crystal, the absorption curves were different due to different morphologies. *Sample A* exhibited a broad absorption peak at 1200 nm (1.03 eV) and a sharp optical absorption locating at 1724 nm (0.72 eV). In contrast to the direct band gap (0.96 eV) of bulk FeS_2, the results showed that the absorption peaks had a blue shift. Other reports showed that band gap of bulk FeS_2 is much larger due to its size effect. *Sample B* didn't show evident absorption peaks and the absorption curve was decreased from 300 nm to 2000 nm. Comparing with *sample B*, the absorption curve of *sample C* and *sample A* showed more similarity due to their similar morphologies. Meantime, the absorption curves of the samples D and E were also different due to different phases (pyrite and marcasite) and morphologies (hollow sphere and rod-like). The hollow sphere marcasite FeS_2 (*Sample D*) had a broad and weak absorption peak at about 1700 nm (0.73 eV) and 1000 nm (1.24 eV), because of a small amount of pyrite FeS_2. In contrast to *sample D*, *sample E* possessed a well-defined, broad optical absorption spanning from 1200 nm to 1600 nm with a distinct peak at 1380 nm (0.90 eV). Optical performance was mainly influenced by its crystal structure, and morphologies, etc.

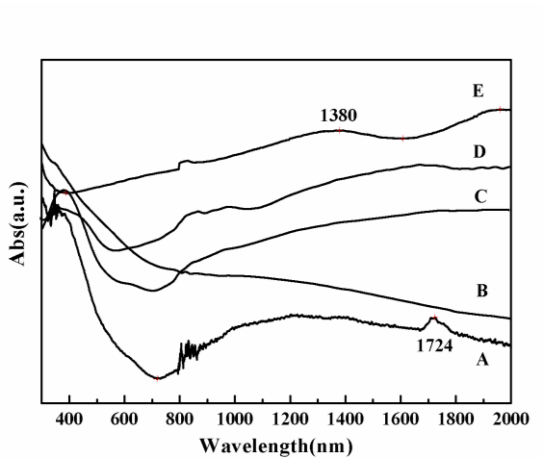

Fig. 11. The UV-vis-NiR absorption spectra of products obtained in the different samples *A, B, C, D, and E.*

Conclusion

In summary, through adjusting of reaction time and volume ratio of ethanolamine and H_2O, pure pyrite FeS_2 crystals with several kinds of morphologies were obtained via hydrothermal process. The hollow sphere of marcasite FeS_2 was synthesis with pure water, the morphology converted to rod-like along with increase of pyrite FeS_2 phase as reaction time lengthened. When $V_{ETA:}V_{H2O}$ was kept at 8:1, the initial flower-like amorphous crystal transformed into flake-like pyrite FeS_2 and then cubic shape. While at 1:8, the flocculent morphologies firstly form into cubic shape, and further transformed into tetrakaidecahedron. At the initial stage of hydrothermal reaction, free Fe^{3+} could coordinate with L-cysteine to form Fe-cysteine precursor which then decomposed to FeS_2 nuclei. The cubic-shape FeS_2 was obtained and then changed owing to the effect of ethanolamine. The absorption properties showed a corresponding change with diverse morphologies, implying that the optical performance was influenced by the structure and morphologies.

Acknowledgment

This work was supported by the financial supports from the Fundamental Research Funds for National Nature Science Foundation of China (51172072, 21237003), Innovation Program of Shanghai Municipal Education Commission (Z2014-070), and the Talent Fund of Shanghai University of Electric Power (K2014-004)

Notes and references

[a] Shanghai Engineering Research Center of Power Generation Environment Protection, Shanghai University of Electric Power, Shanghai 200090, P. R. China

[b] The State Key Laboratory of Safety Science of Pressurized System, School of Mechanical and Power Engineering, East China University of Science and Technology, Shanghai 200237, P. R. China

* E-mail of corresponding author: luan@ecust.edu.cn; Fax: +86 21 6425 3513

(1) W. Y. Kim, Y. C. Choi, S. K. Min and K. S. Kim, *Chem. Soc. Rev.*, 2009, **38**, 2319.

(2) S. Kumar and T. Nann, *Small*, 2006, **2**, 316.

(3) G. D. Scholes, *Adv. Funct. Mater.*, 2008, **18**, 1157.

(4) P. Altermatt, T. Kiesewetter, M. Kunst and H.Tributsch, *Sol. Energy Mater. Sol. Cells*, 2002, **71**, 181.

(5) C. Wadia, A. P. Alivisatos and D. M. Kammen, *Environ. Sci. Technol.*, 2009, **43,** 2072.

(6) Y. Y. Lin, D. Y. Wang, H. C. Yen, H. L. Chen, C. C. Chen, C. M. Chen, C. Y. Tang and C. W. Chen, *Nanotechnology*, 2009, **20,** 405207.

(7) L. A. Montoro and J. M. Rosolen, *Solid State Ionics*, 2003, **159**, 233.

(8) S. B. Lalvani and M. Shami, *J. Electrochem. Soc.*, 1986, **133**, 1364.

(9) S. Ogawa, *J. Appl. Phys.*, 1979, **50**, 2308.

(10) A. Ennaoui, S. Fiechter, C. Pettenkofer, N. Alonsovante, K. Buker, M. Bronold, C. Hopfner and H. Tributsch, *Sol. Energy Mater. Sol. Cells*, 1993, **29(4)**, 289.

(11) C. Wadia, Y. Wu, S. Gul, S. K. Volkman, J. H. Guo and A. P. Alivisatos, *Chem. Mater.*, 2009, **21**, 2568.

(12) J. Puthussery, S. Seefeld, N. Berry, M. Gibbs and M. Law, *J. Am. Chem. Soc.*, 2011, **133,** 716.

(13) D. W. Wang, Q. H. Wang and T. M. Wang, *CrystEngComm.*, 2010, **12,** 755.

(14) Y. Bi, Y. B. Yuan, C. L. Exstrom, S. A. Darveau and J. S, Huang, *Nano Lett.*, 2011, **11**, 4953.

(15) Y. X. Bai, J. Yeom, M. Yang, S. H. Cha, K. Sun and N. A. Kotov, *J. Phys. Chem. C*, 2013, **117(6)**, 2567.

(16) B. X. Yuan, W. L. Luan and S. T. Tu, *Dalton Trans.*, 2012, **41**, 772.

(17) B. X. Yuan, W. L. Luan and S. T. Tu, *CrystEngComm.*, 2012, **14**, 2145

(18) H. J. Fan, U. Gösele and M. Zacharias, *Small*, 2007, **3(10)**, 1660.

(19) J. Li and H. C. Zeng, *J. Am. Chem. Soc.*, 2007, **129**, 15839.

(20) Y. D. Yin, R. M. Rioux, C. K. Erdonmez, S. Hughes, G. A. Somorjai and A. P. Alivisato, *Science*, 2004, **304**, 711.

(21) P. W. Voorhees, *J. Stat. Phys.*, 1985, **38**, 231.

(22) M. Blanchard, M. Alfredsson, J. Brodholt, G. D. Price, K. Wright and C. R. A. Catlow, *J. Phys. Chem. B*, 2005, **109**, 22067.

(23) M. Y. C. Teo, S. A. Kulinich, O. A. Plaksin and A. L. Zhu, *J. Phys. Chem. A*, 2010, **114**, 4173.

The table of contents

Through adjusting of the volume ratio of ETA and H_2O, cubic, flake-like, tetrakaidecahedron, hollow sphere, and rod-like are observed.